

Magnetorefectivity of the inversion layer on *p*-PbTe in the far infrared*

H. Schaber and R. E. Doezema[†]

Physik-Department, Technische Universität München, 8046 Garching, Federal Republic of Germany

(Received 7 June 1979)

From an analysis of magnetorefectance at 119 μm , we obtain values for electron densities, cyclotron masses, and scattering rates in the inversion-layer subbands on *p*-PbTe. The results for the subband densities are in qualitative agreement with the predictions of a simple triangular-well model. Spin resonance of inversion-layer electrons is also observed. A study of cyclotron resonance in magnetic fields tilted with respect to the sample normal shows the dominance of Landau quantization over the electric-subband quantization for motion perpendicular to the surface.

I. INTRODUCTION

Fixed-density space-charge layers were reported for PbTe surfaces some years ago.^{1,2} More recently, variable-density layers were induced on *p*-PbTe using a simple *M-I-S* (metal-insulator semiconductor) arrangement, and Shubnikov-de Haas (SdH) oscillations of bound inversion-layer electrons were observed.³ The dc conductivity value and the SdH value for the induced electron density were not consistent, however. Subsequent to the dc work, a preliminary report of far-infrared magnetorefectance measurements on the *p*-PbTe space-charge system appeared,⁴ and a possible explanation for the density discrepancy was suggested. Here we shall offer firm evidence for the correctness of this explanation.

This evidence results from an analysis of cyclotron resonance of inversion-layer electrons. In the prototype space-charge system Si cyclotron resonance (CR) has been shown to be a valuable probe.⁵ In addition to our CR results, we report the observation of spin resonance in the PbTe inversion layer and show, for motion perpendicular to the surface, that Landau quantization can dominate the usual electric quantization.

These effects occur in PbTe because of the high static dielectric constant $\epsilon_s \sim 1000$ and because PbTe is a narrow-gap semiconductor. In the latter respect, it is joined by InSb (Ref. 6) and HgCdTe (Ref. 7) as narrow-gap semiconductors where inversion-layer CR has been observed. In contrast to these systems, however, PbTe is a multivalley semiconductor with fundamental gap at the *L* points of the Brillouin zone.⁸ The high ϵ_s value reflects the unusual lattice properties of the lead salts: in PbTe, the reststrahlen band is very wide with TO-phonon frequency of $\sim 18 \text{ cm}^{-1}$ and LO-phonon frequency of $\sim 114 \text{ cm}^{-1}$.

The plan of the paper is as follows. Section II contains a brief description of the experiment and

samples. Following this, we discuss the inversion-layer band structure and describe the classical magneto-optical line-shape calculations. Then, before presenting the detailed analysis of the experimental results, we give a general description of the CR, spin-resonance, and tilted-magnetic-field data. Section VI outlines some directions for future work.

II. EXPERIMENTAL DETAILS

Our samples were (111) plane, *p*-type, epitaxial layers grown on BaF₂ substrates.⁹ Sample thicknesses ranged from 5 to 15 μm and their bulk concentrations from $p \sim 4 \times 10^{16}$ to $4 \times 10^{17} \text{ cm}^{-3}$. These nominal concentrations (PbTe is degenerate) were measured as described in Ref. 10.

The *M-I-S* condenser was a sandwich arrangement formed by the sample (area $\sim 5 \times 5 \text{ mm}^2$), a 3.5 μm thick mylar foil, and a semitransparent layer of NiCr evaporated onto the foil. The gate voltage V_G was applied between the NiCr layer and the sample. Contact to the NiCr layer was made with silverprint; a spot of indium evaporated onto the sample provided the second contact. The net induced charge concentration is given by the condenser formula

$$N_{\text{ind}} = \frac{\epsilon_M V_G}{4\pi e d_M}, \quad (1)$$

where ϵ_M and d_M are the static dielectric constant and thickness of the mylar foil, respectively. With V_G in volts, the formula reduces to $N_{\text{ind}} = 4.7 \times 10^9 (V_G) \text{ cm}^{-2}$. The maximum gate voltage which can be applied is about 1000 V; the maximum induced charge concentration is therefore about $5 \times 10^{12} \text{ cm}^{-2}$.

Most of our measurements were performed in the Faraday geometry, i.e., with magnetic field \vec{H} normal to the sample plane. The far-infrared radiation was provided by a gas laser, and standard light-pipe optics were used. It was highly

advantageous to use circularly polarized radiation; the sample was therefore placed in a circular-polarizer unit located within the superconducting magnet. The reflectivity (at 4.2 K) of the sample was measured since, for the frequency used ($\lambda = 118.6 \mu\text{m}$), the transmission of the M - I - S sandwich was low due to reststrahlen-band reflection. The circular-polarizer reflectometer¹¹ was an arrangement of a linear polarizer and a quarter-wave plate. The degree of polarization was high: At $119 \mu\text{m}$, the unwanted mode was seen at the detector (a Ga-doped Ge bolometer) with only $\sim 2\%$ of the intensity of the wanted mode.

Experimentally, we measured the change in sample reflectivity as the gate voltage was square-wave modulated between two fixed values V_1 and V_2 and swept the magnetic field. We thus measured $\Delta R(H) = R_{V_2}(H) - R_{V_1}(H)$; typically, V_2 is a voltage above inversion threshold, and V_1 is chosen near or slightly below threshold.

III. THEORETICAL BACKGROUND

In this section we outline the framework within which we have interpreted our magnetoreflexion data. We describe the application of the Stern-Howard¹² picture to obtain the subband dispersion in the two-dimensional inversion layer:

$$E_i(k_x, k_y) = E_i + \hbar^2 k_x^2 / 2m_x + \hbar^2 k_y^2 / 2m_y. \quad (2)$$

The energies E_i result from the electric-field-induced quantization normal to the surface (z direction), and the remaining terms describe the motion along the sample surface. We discuss first the parallel motion, i.e., the determination of m_x and m_y , and then turn to the subband-edge energies E_i . In the last part of this section, we present the classical line-shape treatment used to analyze the data.

A. Bulk and surface band structure

The direct, fundamental energy gap has the value $E_g = 0.190 \text{ eV}$ at 4.2 K and occurs at the L points of the Brillouin zone for PbTe. The corresponding surfaces of constant energy for both valence and conduction bands consist of four elongated ellipsoids along the $\langle 111 \rangle$ directions. Therefore, with respect to the plane of the sample surface, there is a single ellipsoid (a) along the z direction and a threefold degenerate set of ellipsoids (b) whose major axes form an angle of 70.53° with the z direction. Each ellipsoid has the transverse and longitudinal mass components m_t and m_l referred to its principle axes. These masses vary with energy, reflecting the nonparabolicity of the PbTe band structure near the L point. At the band minima, we take the values

$m_t = 0.0213m_0$ and $m_l = 0.21m_0$ (corresponding valence-band maxima values are $0.0232m_0$ and $0.26m_0$) to agree with the bulk CR we observe in our samples. (The uncertainty associated with the m_t values is about $\pm 2.5\%$ and with the m_l values about $\pm 5\%$ and $\pm 10\%$ for conduction and valence bands, respectively.) Our values are in good agreement with those of Appold *et al.*¹³

For determining the two-dimensional, inversion-layer band structure, we use the results of Stern and Howard.¹² Two subband systems arise: one from the a ellipsoid, the other from the b ellipsoids. The lines of constant energy in k space corresponding to the two-dimensional (2-D) motion are found by projecting the three-dimensional (3-D) surfaces of constant energy onto the plane of the sample surface. For the a ellipsoid, one thus obtains circles of constant energy with mass components $m_x = m_y = m_t$, and for the b ellipsoids, one gets ellipses of constant energy with mass components m_t and $\frac{1}{3}(m_t + 8m_l)$. Thus, the expected 2-D cyclotron mass $(m_x m_y)^{1/2}$ is given for the a ellipse by $m_{c,s}^a = m_t$ as in the bulk and for the b ellipses by

$$m_{c,s}^b = \frac{1}{3}m_t(1 + 8m_l/m_t)^{1/2}, \quad (3)$$

which is larger than the corresponding volume mass

$$m_{c,v}^b = 3m_t(1 + 8m_l/m_t)^{-1/2}. \quad (4)$$

B. Subband energies and occupations

In general, to find the quantized energies and subband occupations, one must solve Poisson's equation and the Schrödinger equation self-consistently.¹⁴ This self-consistency problem is usually complicated (e.g., in Si) by many-body and image-potential corrections. In PbTe, due to the small effective masses and the high dielectric constant, one expects such corrections to be negligible. The high ϵ_s value and the relatively high bulk carrier concentrations p also allow us, as a reasonable approximation, to neglect the self-consistent aspect of the charge-layer problem.¹⁴ In this section, we outline how this comes about and give the resulting subband energies and occupations.

As a visual guide for the following discussion, we show, in Fig. 1, the schematic band-bending picture which applies to inversion on p -PbTe. The density of depletion charge at inversion threshold is given by

$$N_d = p z_d = (\epsilon_s p E_g / 2\pi e^2)^{1/2}, \quad (5)$$

where z_d is the depletion length at threshold. Taking $\epsilon_s = 1300$ (Ref. 15), we thus have $N_d \cong 3 \times 10^{12} \text{ cm}^{-2}$ and $z_d \cong 0.8 \mu\text{m}$ for the lowest of our

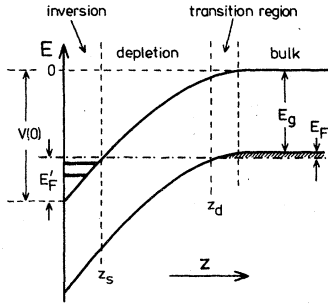


FIG. 1. Schematic view of the band bending for an inversion layer on p -PbTe.

bulk concentrations, $p = 4 \times 10^{16} \text{ cm}^{-3}$. Since our maximum net induced charge is typically $5 \times 10^{12} \text{ cm}^{-2}$, we usually have the inversion density N_s less than the depletion density even for our lowest volume concentrations.

For $N_s \leq N_d$ and $z \sim z_s \ll z_d$, one obtains, after twofold integration of the Poisson equation, the potential $V(z)$ near the surface [for $V(\infty) = 0$]:

$$V(z) \cong -2\pi e^2 N_d z_d / \epsilon_s + (4\pi e^2 / \epsilon_s) (N_d + N_s) z. \quad (6)$$

We are thus neglecting the curvature of the potential due to the inversion charge, removing the coupling to the Schrödinger equation. A less serious approximation is our neglect of the transition region in Fig. 1.¹⁴ Taking the potential barrier at the surface as infinite, we thus have the well-known triangular-well problem. The wave-function solutions of the Schrödinger equation are the Airy functions; the corresponding energy eigenvalues are, to an excellent approximation, given by¹⁴

$$E_{ij} = \left(\hbar \frac{\partial V}{\partial z} \right)^{2/3} (2m_1^j)^{-1/3} \left[\frac{3}{2}\pi \left(i + \frac{3}{4} \right) \right]^{2/3} \quad (7)$$

$$(i = 0, 1, 2, \dots),$$

where $j = a$ or b , and m_1 is the mass component for the z direction from the bulk dispersion. The a ellipsoid (with $m_1^a = m_1$) thus gives rise to the subband-edge energies E_{0a}, E_{1a}, \dots and the b ellipsoids with $m_1^b = 9m_1 m_1^b (m_1^b + 8m_1)^{-1}$ to the threefold degenerate set E_{0b}, E_{1b}, \dots . These subband sets are often referred to as the unprimed and primed set, respectively.

Through (6), the inversion density is related to the field in the semiconductor:

$$N_s = \frac{\epsilon_s}{4\pi e^2} \frac{\partial V}{\partial z} - N_d. \quad (8)$$

With use of the usual 2-D expression for the density of states and neglecting nonparabolic effects, it is also given by

$$N_s = \sum_{i,j} \frac{g_j m_{c,s}^3}{\pi \hbar^2} (E'_F - E_{ij}) \Theta(E'_F - E_{ij})$$

$$\cong \sum_{i,j} N_{ij}. \quad (9)$$

Here, g_j is the valley degeneracy $g_a = 1$ and $g_b = 3$. The energy E'_F is the Fermi energy measured from the bottom of the triangular well. It is related to the bulk Fermi energy measured from the top of the valence band and to the total band bending $V(0)$, as in Fig. 1, by

$$E'_F = (2\pi e^2 / \epsilon_s) N_d z_d - (E_g + E_F). \quad (10)$$

Setting (8) equal to (9) and using (7) and (10) yields a quadratic equation for N_d with $\partial V / \partial z$, i.e., $N_{\text{ind}} = N_s + N_d$, as parameter. The results for $p = 4 \times 10^{16} \text{ cm}^{-3}$ and $\epsilon_s = 1300$ are shown in Fig. 2, where we have plotted subband energies E_{ij}, E'_F , and subband occupations N_{ij} vs N_{ind} . Assuming no intrinsic surface charge, we may simply relate N_{ind} to the applied gate voltage through Eq. (1).

A final point of interest in this section is the thickness of the inversion layer. The classical turning points range from $\sim 100 \text{ \AA}$ for the lowest occupied ($0a$) subband to $\sim 500 \text{ \AA}$ for the highest occupied ($5a$) subband shown in Fig. 2. The thickness is thus typically an order of magnitude larger than usually encountered in Si.

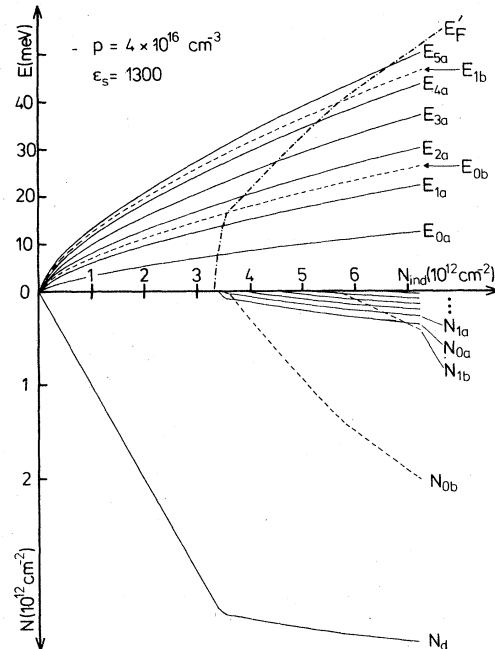


FIG. 2. Subband energies and densities versus induced charge (relative to the flatband condition) from the triangular-well model.

C. Magneto-optical line-shape calculations

To calculate the reflectivity of our samples in the presence of a magnetic field, we need to describe the optical response of the sample sandwich pictured schematically in Fig. 3. For the wavelengths of interest here, the effect of the mylar insulator and NiCr gate may be safely neglected, the BaF₂ (thickness ~0.5 mm) can be considered as infinitely thick, and the inversion layer can be treated as infinitely thin. The reflectivity problem is thus reduced to the double-layer problem with media 1, 2, 3, and 4, in Fig. 3, which includes an altered boundary condition¹⁶ due to the inversion layer at the interface between media 1 and 2. The calculation is straightforward, and the results are contained elsewhere.¹⁷

In the calculation, we assume that the response of each sample component to the incoming radiation in the presence of the magnetic field H is governed by a classical, local-limit, dielectric tensor of the form

$$\vec{\epsilon}(\omega, \vec{H}) = \vec{\epsilon}_L(\omega) + \vec{\epsilon}_{fc}(\omega, \vec{H}). \quad (11)$$

For the lattice part $\epsilon_L(\omega)$, we take the standard oscillator model with parameters as given by Burkhard *et al.*¹⁵ The free-carrier part $\epsilon_{fc}(\omega, \vec{H})$ has been given for the bulk for propagation direction $\vec{q} \parallel \vec{H} \parallel \langle 111 \rangle$ in the Faraday geometry by Wallace¹⁸ and is also contained in Ref. 15. The dielectric tensor is written most simply in terms of circular-polarization components ϵ^* describing the CR active and inactive modes. We refer to these modes as hole active and electron active. The parameters entering ϵ^* are the bulk carrier concentration p (which is subdivided into a and b contributions), the mass components m_a and m_b (yielding the a and b cyclotron masses), and relaxation time parameters τ_a and τ_b for both ellipsoid systems. These determine the response of layer 3 in Fig. 3.

The response for the depletion layer, region 2, is simple: In the absence of free carriers, $\vec{\epsilon}(\omega, \vec{H})$ reduces to $\vec{\epsilon}_L(\omega)$. The dielectric function ϵ_{2-D}^* for the inversion layer is formally the same

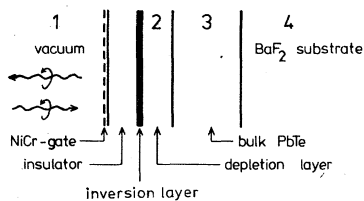


FIG. 3. *M-I-S* sandwich arrangement for the PbTe epitaxial layers.

as the free-carrier response for the bulk; the bulk density p is replaced by the 2-D densities N_{ij} , the bulk cyclotron mass parameter by a subband cyclotron mass, and the bulk relaxation time parameter by a relaxation time for each subband. The ϵ^* functions for each subband contribute additively to the total ϵ_{2-D}^* .

The depletion length and the PbTe thickness also enter the reflectivity and can be considered as fit parameters. We thus have, in principle, an enormous number of parameters available. In practice, as we see below, the bulk parameters have little influence on the determination of the inversion-layer parameters, and for these we make certain additional simplifying assumptions.

IV. SURVEY OF EXPERIMENTAL RESULTS

The purpose of this section is to introduce and characterize the CR of inversion carriers in PbTe. We also present our observation of the spin resonance of the inversion carriers and discuss the result of tipping and magnetic field out of the Faraday geometry.

A. Cyclotron resonance at 119 μm

1. Circular polarization

Inversion is easily demonstrated by transistor action in samples with source-drain contacts.³ The "masking" effect⁴ in the reststrahlen band gives another clear indication of inversion in the far-infrared magnetoreflexivity. Here, the highly reflecting depletion layer (real part of $\epsilon_L = -30$ at 119 μm) masks the CR from the bulk, isolating the inversion CR.

An elegant way to demonstrate inversion in our degenerate samples is to use circular polarization. For circular orbits, electrons and holes exhibit CR in opposite modes. Thus, for example, CR associated with the a valley will be seen in the electron active mode for n inversion, and in the hole-active mode for bulk carriers. This is illustrated in Fig. 4. The figure also exhibits the masking effect in the hole-active mode along with the accumulation signals discussed in Ref. 4. The masking effect in principle provides a determination of the depletion length z_d ; this, together with the depletion density N_d (from the flatband to threshold voltage $V_{th} - V_{FB}$), provides a far-infrared determination of ϵ_s and p from Eq. (5).

For the b valleys, bulk and inversion signals can appear in both polarization modes since the orbits are elliptical. At 119 μm , however, the masking severely reduces the bulk CR signal in the presence of the full depletion layer.

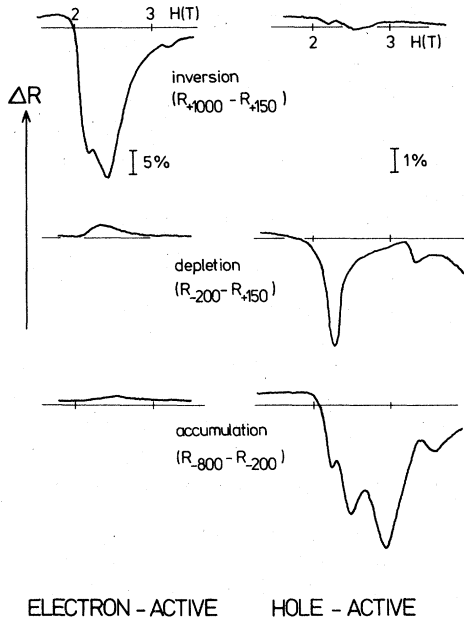


FIG. 4. Differential magnetorelectance at $119 \mu\text{m}$ at the a -valley resonance in both modes of circular polarization for a (111) PbTe sample with $p \approx 4 \times 10^6 \text{ (cm)}^{-3}$. As the gate voltage is chopped between $+1000 \text{ V}$ and the threshold voltage ($+150 \text{ V}$), only the inversion signal is seen. From threshold to flatband (-200 V), only the bulk hole cyclotron resonance is seen ("masking"). Chopping from flatband into accumulation produces new hole mode structure.

2. General features

The differential reflectivity ΔR in the electron-active mode over the magnetic field range $0\text{--}7 \text{ T}$ is shown in Fig. 5. This series of ΔR traces is for a sample where the threshold gate voltage V_{th} was about $+150 \text{ V}$. The reference gate voltage V_1 was held at 0 V and the upper voltage V_2 was varied in steps deep into inversion.

The structure just above 2 T is CR of a valley inversion electrons, as is also shown in Fig. 4. At the highest gate voltages, it is composed of a multiplet of closely spaced peaks. Such multiplets are familiar from inversion CR in InSb (Ref. 6) and arise in a nonparabolic system in which a slightly different cyclotron mass is observed for each occupied subband.

A second important feature is the structure at 5 T . This is the CR signal of b valley inversion electrons. The lowest b subband becomes occupied very near threshold as predicted by the calculation of Fig. 2. Occupation of the b system was also suggested in Ref. 4 as a possible explanation for the low carrier densities observed in the SdH work.³

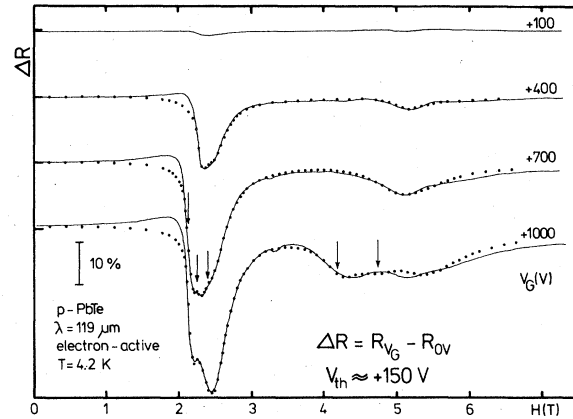


FIG. 5. Experimental (solid curves) and calculated (dotted curves) differential magnetorelectivity of the PbTe inversion layer. The short markers on the left denote the $\Delta R = 0$ values for each curve. The arrows denote the assumed resonance positions for the fit.

B. Spin resonance

A third general feature in Fig. 5 is the small dip just above 3 T which is visible above $V_G \approx +700 \text{ V}$. This we ascribe to spin resonance (SR) of inversion-layer electrons.

Electric-dipole-electron spin resonance (EDE-ESR) occurs in bulk narrow-gap semiconductors because of band nonparabolicity.^{19,20} Lack of inversion symmetry can also cause EDE-ESR,²¹ and it is essentially this mechanism, via the surface potential, which Därr *et al.*²² suggest is responsible for EDE-ESR in the InSb inversion layer.

It was only very recently that we reported the observation of EDE-ESR in bulk PbTe.²³ Line-shape aspects in PbTe as well as in other narrow-gap materials are incompletely understood; thus, it is not surprising that the situation in the inversion layer is no better. Our purpose in this section is merely to point out certain experimental features of inversion-layer SR in PbTe. Much remains to be clarified experimentally and theoretically.

To enhance the SR signal, we detect the field derivative dR/dH of the reflectivity and sweep H for various constant values of gate voltage as in Fig. 6 (for a different but similar sample).

The resonance becomes visible at $V_G - V_{\text{th}} \approx 600 \text{ V}$, suggesting that we are observing SR of a higher subband. This is substantiated by the apparently additional structure appearing near $V_G - V_{\text{th}} \approx 1000 \text{ V}$, indicating a possible next higher subband. That the amplitudes appear to be different is reminiscent of InSb,²² where the amplitude variation between EDE-ESR from different subbands is related by theory to the differ-

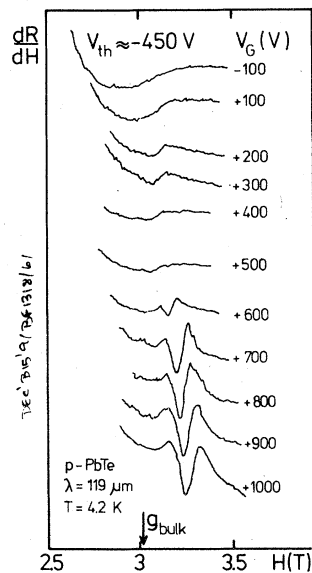


FIG. 6. Inversion-layer spin resonance in PbTe. The polarization mode is electron active. The spin-resonance position corresponding to the bulk conduction-band-edge g factor is marked.

ent depths z_i for each subband. The disappearance of the resonance near $V_G - V_{th} \approx 900$ V is a phenomenon also observed in InSb (Ref. 24). In a completely quantized system, SR is not possible when the spin-up and spin-down states corresponding to a given Landau level are either both full or both empty.

The SR position expected from the conduction-band-edge value of the bulk g factor²³ is indicated in Fig. 6. The slightly higher resonance fields in the inversion layer (i.e., slightly lower g factors) and the slight variations of the positions with V_G can be ascribed to nonparabolic effects as in the work of Därr *et al.* The widths of the resonances are also comparable to InSb.

There are, however, at least two notable differences with EDE-ESR in InSb. The inversion-layer SR in PbTe is seen only in the electron-active mode. (Any possible signal below the noise in the inactive mode is at most 10% of the active-mode signal.) In contrast, no polarization dependence was found in InSb—as predicted by theory.²² A second difference is that, upon tipping the magnetic field away from the sample normal, we find little or no variation in SR amplitude for up to 50° tilt. In InSb, an increase by a factor of 20 in signal amplitude was observed when tilting from 0° to 45° .

Perhaps the clue to the deviant behavior in PbTe is to be found in the 3-D nature of the PbTe inversion layer in a magnetic field. This is the subject of Sec. III C.

C. Three-dimensional behavior

One of the standard tests for the quasi-2-D space-charge layer is CR in a magnetic field tipped away from the sample normal.¹⁶ The motion of the 2-D gas is expected to be sensitive only to the normal component of the field, so that the resonance position shifts to higher fields as $(\cos\theta)^{-1}$, where θ is the tilt angle. Let us examine the PbTe resonances in tilted fields. (For this we arranged the sample in a split-coil magnet to permit continuous tilt variation.)

As tilting commences, the b resonance breaks up into three distinct peaks as seen in Fig. 7. For the given direction of tilt (Fig. 7), this is the behavior expected for bulk CR, where the triple degeneracy of the cyclotron mass is broken by tipping. The splitting is a dramatic departure from the 2-D $(\cos\theta)^{-1}$ behavior.

For large tipping angles, the departure from the $(\cos\theta)^{-1}$ variation also becomes apparent for the a valley. Figure 8 shows the variation of the peak positions over the whole 90° range from Faraday to Voigt geometry. Also shown are the tilting results for bulk CR in an n -type sample. The agreement between the bulk and surface peak positions and the mass variation expected from the ellipsoidal model for volume CR is convincing evidence that the quasi-2-D layer is exhibiting 3-D characteristics in a magnetic field. This is not at all unexpected.

For simplicity, we consider the Voigt geometry ($\theta = 90^\circ$). In the strictly 2-D picture, no CR can take place, i.e., the magnetic force in the z direction has no influence on the quantization due to the electric field. In the quasi-2-D surface layers, however, the Landau quantization may dominate the electric quantization. This condition occurs roughly when the semiclassical turn-

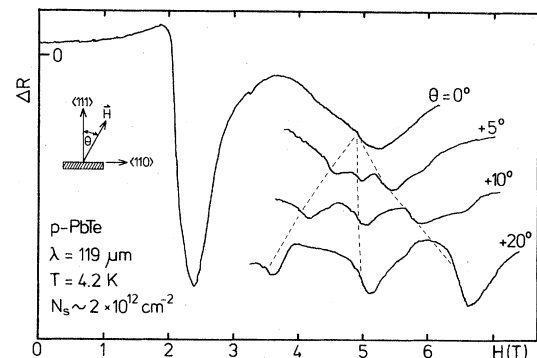


FIG. 7. Change of the b -valley inversion-layer resonance as the magnetic field is tilted from the sample normal.

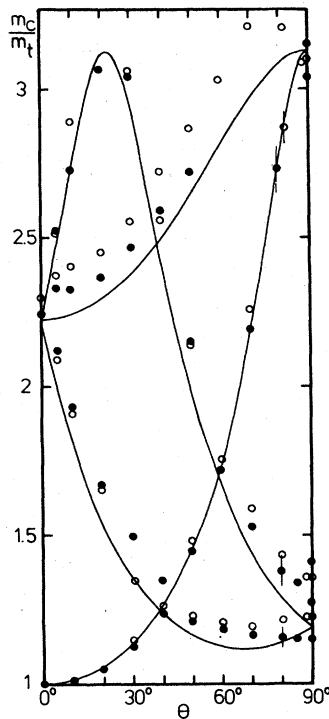


FIG. 8. Variation of inversion-layer (closed circles) and n -type bulk (open circles) CR peak positions versus tip angle θ . The positions are normalized to the resonance condition for the a valley (mass m_t). The solid line is the bulk cyclotron mass variation expected for $m_1/m_t = 9.8$.

ing points in the magnetic potential lie between the turning points corresponding to the electric potential, i.e.,

$$2R_c(\eta) < z_i, \quad (12)$$

where $R_c(\eta)$ is the cyclotron radius. Whether or not the above condition is satisfied depends on Landau index n , subband index i , and (through z_i) on the applied electric field, i.e., on $N_s + N_d$. The condition (12) is satisfied in PbTe except for the lowest a subbands and higher ($\eta \geq 3$) Landau levels. A more careful analysis¹⁷ shows that the above condition is too rigid. The analysis is based on the semiclassical Bohr-Sommerfeld quantization. The form of the equation of motion is not altered by inclusion of the electric potential so that numerical methods²⁵ can be utilized for the crossed electric and magnetic field case as shown by Beinvogl *et al.*²⁶ The Bohr-Sommerfeld approach gives results which closely approximate the more exact results of Ando.²⁷ Bulklike CR is expected for $H \geq 1$ T, as we observe.

For geometries other than Voigt and in the Faraday geometry for ellipsoids tilted with respect to the sample surface, an analytical calculation be-

comes exceedingly cumbersome. Nevertheless, a comparison of magnetic and electric lengths shows that, for such situations, 3-D behavior in magnetic fields is expected. Thus, even in the Faraday geometry, the CR of the b valleys is 3-D-like (i.e., tilted orbits) as is evidenced by the splitting of the b signal even for small tilt angles.

V. DETAILED ANALYSIS

In this section, we use the results of fitting and magneto-reflection line-shapes to obtain occupation densities N_s , cyclotron masses m_c , and relaxation times τ for the surface subbands. Representative fits are shown in Fig. 5. For the a -valley resonance, we assume up to three subbands (as visual inspection suggests) even though our calculation (Fig. 2) predicts more. (Even at the lowest V_G values, the a resonance probably arises from two subbands.)

The two peaks at higher fields are identified and fit as corresponding to the $0b$ and $1b$ subbands. For a single, isolated subband, N_s is related to the integrated intensity of the resonance, m_c to its position, and τ to its width; thus, in principle, all three parameters are independent.

As may be judged from Fig. 5, the fit results are generally good with two exceptions: the low-field side of the a resonances and the high-field side of the b resonances. We have no explanation for the first discrepancy; perhaps it represents a failure of the classical linefitting. The b resonance discrepancy is likely due to the 3-D effects discussed above. The subband edges for the tilted b ellipsoids will no longer correspond to the simple, electric E_{ib} values in strong magnetic fields, and the observed CR will be bulklike. This is confirmed by the observed b masses, which take on bulk rather than the $\sim 30\%$ higher 2-D values. The Landau-level spacing is then not completely uniform as a function of orbit center position. Thus the observed line should be inhomogeneously broadened in contrast to our calculated, single-resonance line, and not all b electrons appear in the peak. With the above remarks in mind, let us consider the results of the fitting.

A. Subband occupations

The previously reported SdH work³ showed only a single set of oscillations corresponding to a single subband, the occupation of which was $\sim 5\%$ of the expected, net-induced charge. It was subsequently suggested⁴ that additional oscillations should have appeared corresponding to multiple

subbands of the a and b valleys. The majority of induced electrons is expected to occupy the b valleys because of their higher mass and degeneracy factor (Fig. 2).

That this explanation is essentially correct is demonstrated by the observation of the b valley resonances. Subband $0b$ is occupied very near threshold, as the calculation (Fig. 2) predicts. A further confirmation is the gate voltage at which the $1b$ signal appears; it is within $\sim 20\%$ of the triangular-well prediction.

As seen in Fig. 9, however, all is not obviously well. By comparison to the triangular-well prediction, the density of a valley electrons is somewhat too high and the b valley density much too low. (The error bars for the N_s values in Fig. 9 amount to about $\pm 15\%$. Half this amount is due to the spread in fit parameters which satisfactorily reproduce the experimental curve and the other half to experimental uncertainty in determining ΔR absolutely.)

The a valley discrepancy is not too alarming. Agreement could be improved by adjusting ϵ_s , p , or both. Furthermore, any shifts of the b subbands, e.g., due to 3-D effects (difficult to estimate since perturbation theory¹² no longer applies) or surface strain effects, will cause redis-

tribution of inversion electrons.

We believe that the remaining charge (aside from a small fraction, $\sim 10\%$, which goes into increasing the depletion charge as in Fig. 2) occupies the b subbands as predicted. The b valley discrepancy of Fig. 9, then, is due to our overly simplified line-shape analysis which ignores 3-D effects.

B. Cyclotron masses

From our line-shape fit, we obtain the masses plotted versus gate voltage in Fig. 10. As noted above, the inversion-layer b electrons have masses lying near the bulk value for the b valley mass (Eq. 4) rather than the 2-D value (Eq. 3) due to the dominance of the magnetic force for the tilted ellipsoids. That the masses for subbands $0b$ and $1b$ differ can be ascribed to nonparabolic effects since the effective Fermi energy $E'_F - E_{ij}$ is different for each subband. The gate voltage dependence of the masses is not understood; it may again be due to 3-D line-shape effects.

The a subbands also show splitting, characteristic of nonparabolicity. The independence on gate voltage of the mass values is, however, not expected (compare the work in InSb, Ref. 6).

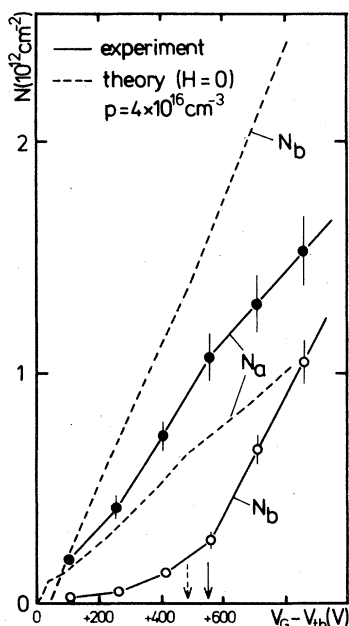


FIG. 9. Inversion-layer densities for a - and b -valley electrons. Experimental values are obtained from line-shape fits as in Fig. 5; calculated values follow from Fig. 2 and Eq. (1). The arrows denote the experimental and calculated gate voltages above which the $1b$ subband is occupied.

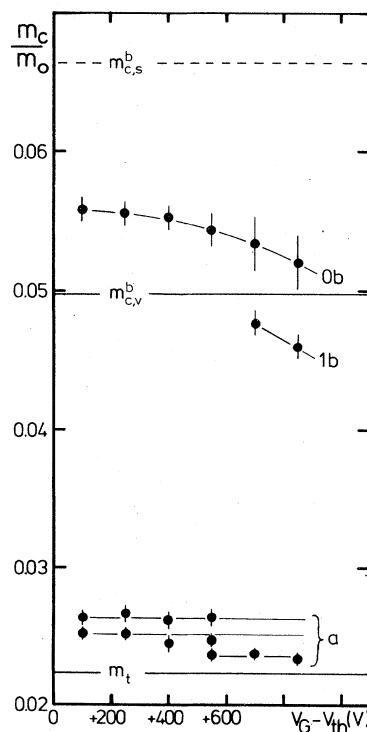


FIG. 10. Inversion-layer cyclotron masses versus gate voltage.

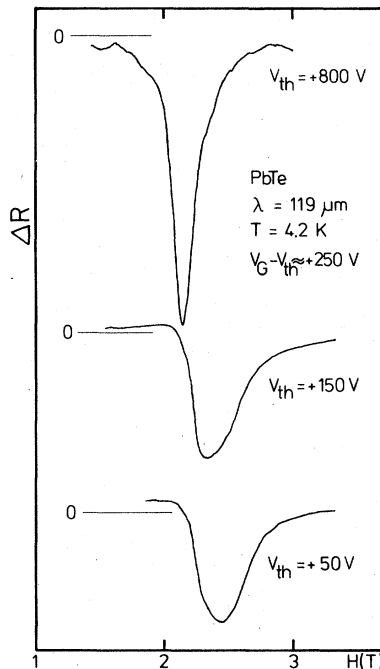


FIG. 11. Variation of inversion-layer CR and threshold voltage with sample condition. The curves are measurements at intervals of eight and two months, respectively, starting at the top.

Thus the extrapolated subband-edge mass values all lie above the corresponding mass m_t at the bottom of the conduction band.

The inversion-layer mass values depend, moreover, on the sample condition. In a single sample, measured at various intervals over a period of a year, the inversion-layer mass was observed to rise about 10% from a value near the conduction-band value. The rise is correlated with a broadening of the line by nearly a factor of 2 and a dramatic decrease in the threshold voltage as indicated in Fig. 11. No change in the flatband to threshold voltage was observed.

Such sample-dependent mass shifts are well known in Si.⁵ Except at low densities where localization effects are responsible, their cause is not fully understood. In PbTe, the mass shifts are a definite surface effect; bulk CR remains unaffected. Contamination of PbTe surfaces is common²⁸; we took no extraordinary precautions in storing the samples—they were stored with the mylar foil in place, in air.

C. Scattering rates

The values for the scattering rate $1/\tau$ obtained from the fits are typically $5 \times 10^{11} \text{ sec}^{-1}$, about three times lower than in InSb (Ref. 24) and about two times lower than typical values in Si.¹⁶ The correspondingly high mobilities in the

PbTe inversion layer have been noted previously³ and are close in value to the excellent bulk mobilities in these PbTe films. The near equality of bulk and surface scattering rates is another manifestation of the relatively thick inversion layers in PbTe, in which the influence of surface scattering is minimized. This is also evidenced by the apparent independence of scattering rate on subband index and density, in contrast to the behavior in InSb and Si.

VI. CONCLUDING REMARKS

With the help of the simple triangular-well model and the classical line-shape description, we have used the far-infrared CR results to characterize the inversion layer on *p*-PbTe. We have accounted for most, if not all, of the induced charge in the form of multiple subband densities, thus solving the puzzle left by the earlier SdH results.³ In addition, the influence of the magnetic field was shown to cause 3-D behavior in the unusually thick PbTe inversion layer. Although these 3-D effects are also thought to be responsible for difficulties in fitting the *b* valley resonances, a proper calculation should be undertaken to support this. Our triangular-well calculation is an $H=0$ calculation and, as such, cannot correctly describe the *b* valley subbands. Extension of the experiments to lower frequencies should show reversion to 2-D character.

This has been a paper about inversion. Only in accumulation, however, are the PbTe space-charge layers expected to exhibit behavior characteristic of a degenerate semiconductor. Little can be added to material already published⁴ concerning accumulation, although, as in inversion, we observe a spin-resonance signal.

The observation and study of intersubband resonance²⁹ would be highly useful in understanding accumulation and in obtaining more quantitative information on the PbTe inversionlayer subbands, with and without a magnetic field. Another area of future interest is a careful analysis of CR near the LO-phonon frequency.¹⁷ Both frequency and temperature variation would be useful for characterization of the scattering in the inversion layer.

VII. ACKNOWLEDGMENTS

This work would not have been possible without the generous help of A. Lopez-Otero in providing the PbTe epitaxial layers. We also wish to express our heartfelt appreciation to F. Koch for his encouragement and interest and useful discussions. Financial support was given by the Deutsche Forschungsgemeinschaft (SFB 128).

- *Based on a doctoral thesis submitted by H. S. in partial fulfillment of the requirements for the degree Dr. rer. nat. at the Technische Universität München.
- [†]New address: Department of Physics and Astronomy, University of Oklahoma, Norman, Oklahoma 73019.
- ¹K. W. Nill, A. R. Calawa, T. C. Harman, and J. N. Walpole, *Appl. Phys. Lett.* **16**, 375 (1970).
- ²D. C. Tsui, G. Kaminsky, and P. H. Schmidt, *Phys. Rev. B* **9**, 3524 (1974).
- ³H. Schaber, R. E. Doezema, P. J. Stiles, and A. Lopez-Otero, *Solid State Commun.* **23**, 405 (1977).
- ⁴H. Schaber, R. E. Doezema, J. F. Koch, and A. Lopez-Otero, *Solid State Commun.* **26**, 7 (1978).
- ⁵J. P. Kotthaus, *Surf. Sci.* **73**, 472 (1978).
- ⁶A. Därr, J. P. Kotthaus, and J. F. Koch, *Solid State Commun.* **17**, 455 (1975).
- ⁷T. Kuroda and S. Narita, *J. Phys. Soc. Jpn.* **41**, 709 (1976).
- ⁸For a review of PbTe properties, see: R. Dalven, in *Solid State Physics*, edited by H. Ehrenreich, F. Seitz, and D. Turnbull (Academic, New York, 1973), Vol. 28.
- ⁹A. Lopez-Otero, D. Duh, and J. N. Zemel, *Mater. Sci. Eng.* **17**, 63 (1975); A. Lopez-Otero, *J. Appl. Phys.* **48**, 446 (1977).
- ¹⁰A. Lopez-Otero, *Appl. Phys. Lett.* **29**, 441 (1976).
- ¹¹H. Schaber and R. E. Doezema, *Infrared Phys.* **18**, 247 (1978).
- ¹²F. Stern and W. E. Howard, *Phys. Rev.* **163**, 816 (1967).
- ¹³G. Appold, R. Grisar, G. Bauer, H. Burkhard, R. Ebert, H. Pascher, and H. G. Häfele, *Proceedings of the XIV International Conference on the Physics of Semiconductors, Edinburgh, 1978* (Institute of Physics, London, 1979), Vol. 43, p. 1101.
- ¹⁴See, for example, F. Stern, *Phys. Rev. B* **5**, 4891 (1972).
- ¹⁵H. Burkhard, G. Bauer, P. Grosse, and A. Lopez-Otero, *Phys. Status Solidi B* **76**, 259 (1976).
- ¹⁶G. Abstreiter, J. P. Kotthaus, J. F. Koch, and G. Dorda, *Phys. Rev. B* **14**, 2480 (1976).
- ¹⁷H. Schaber, Doctoral dissertation, Technische Universität, München, 1979 (unpublished).
- ¹⁸P. R. Wallace, in *Physics of Solids in Intense Magnetic Fields*, edited by E. D. Haidemenakis (Plenum, New York, 1969), p. 73.
- ¹⁹V. I. Sheka, *Fiz. Tverd. Tela (Leningrad)* **6**, 3099 (1964) [*Sov. Phys. Solid State* **6**, 2470 (1965)].
- ²⁰B. D. McCombe, *Phys. Rev.* **181**, 1206 (1969).
- ²¹E. I. Rashba and V. I. Sheka, *Fiz. Tverd. Tela (Leningrad)* **3**, 1735 (1961) [*Sov. Phys. Solid State* **3**, 1257 (1961)].
- ²²A. Därr, J. P. Kotthaus, and T. Ando, *Proceedings of the XIII International Conference on the Physics of Semiconductors, Rome, 1976*, edited by F. G. Fumi (North-Holland, Amsterdam, 1976), p. 774.
- ²³H. Schaber and R. E. Doezema, *Solid State Commun.* **31**, 197 (1979).
- ²⁴A. Därr, Doctoral dissertation, Technische Universität München, 1978 (unpublished).
- ²⁵M. Wanner, R. E. Doezema, and U. Strom, *Phys. Rev. B* **12**, 2883 (1975).
- ²⁶W. Beinvoogl., A. Kamgar, and J. F. Koch, *Phys. Rev. B* **14**, 4274 (1976).
- ²⁷T. Ando, *J. Phys. Soc. Jpn.* **39**, 411 (1975).
- ²⁸G. M. T. Foley and D. N. Langenberg, *Phys. Rev. B* **15**, 4830 (1977).
- ²⁹F. Koch, *Surf. Sci.* **80**, 110 (1979).